Korean J. Chem. Eng., 36(3), 377-384 (2019)
DOI: 10.1007/s11814-018-0227-9

pISSN: 0256-1115
eISSN: 1975-7220

Regeneration of commercial SCR catalyst deactivated by arsenic poisoning in coal-fired power plants

Qiang Lu*,†, Zulfiqar Ali*, Hao Tang*, Tahir Iqbal*, Zulqarnain Arain, Min-shu Cui*, Ding-jia Liu*, Wen-yan Li*, and Yong-ping Yang***

*National Engineering Laboratory for Biomass Power Generation Equipment, North China Electric Power University, Beijing 102206, China
**Department of Energy System Engineering, Sukkur IBA University, Sukkur, Pakistan
(*Received 23 October 2018 • accepted 14 January 2019*)

Abstract–Arsenic species, which are inevitable components in flue gas from the coal combustion process, will result in severe deactivation of selective catalytic reduction (SCR) catalysts. In this paper, a novel method is proposed to regenerate the arsenic-poisoned commercial V_2O_5-MoO_3/TiO_2 catalyst collected from coal-fired power plants, including ammonia washing, H_2 reduction, and air calcination. Activity tests indicated that the proposed method could recover the catalyst activity more than 96% of the fresh catalyst. Furthermore, detailed characterizations results indicated that this regeneration method could not only effectively remove the arsenic species, but also recover the active constituents of the catalysts to a considerable level. The proposed method offers a feasible strategy for the regeneration of poisoned commercial SCR catalysts and can effectively reduce the total denitrification cost for coal-fired power plants.

Keywords: SCR Catalyst, Deactivation, Regeneration, Arsenic, V_2O_5-MoO_3/TiO_2

INTRODUCTION

Selective catalytic reduction (SCR) with ammonia as a reducing agent is the most successful and commercialized technology for abating NO_X emission from coal-fired power plants [1-4]. The widely employed catalyst in the NH_3-SCR system was honeycomb or plate type V_2O_5-WO_3(MoO_3)/TiO_2 with V_2O_5 as the active phase, WO_3(MoO_3) as the chemical promoter and TiO_2 as the carrier [5-7]. Some of the flue gas components from the coal combustion process can be a serious threat to the normal operation of the SCR system. SO_2, alkali metals (e.g., K, Na) and heavy metals (e.g., As, Pb and Hg) in flue gas usually cause severe deactivation of SCR catalyst, shortening the catalyst lifespan [8-12]. The regeneration of deactivated SCR catalysts will provide significant benefits in both economical and environmental aspects, due to the decrease in the cost of denitrification and solid wastes recycling for power plants [13,14]. Various studies have been performed to regenerate different deactivated SCR catalysts, mainly focusing on catalysts poisoned by alkali metals or acidic gas. However, limited attention has been paid to the regeneration of SCR catalysts poisoned by heavy metals.

Arsenic is a toxic trace element in coal, the concentration of arsenic species in coal-fired flue gas ranges from 1 $\mu g/m^3$ to 10 mg/m^3 [15], mainly in the form of arsenopyrite (FeAsS), which can be oxidized to As_2O_3 during combustion. It has been reported that arsenic species would cause serious deactivation of the SCR catalyst [16,17]. Generally, gaseous As_2O_3 can diffuse into the catalyst and clog its micropores through the siphon effect. Specifically, when the partial pressure of As_2O_3 exceeds its partial equilibrium pressure, it will condense and cover the acid sites of the catalyst [15]. In addition, the adsorbed As_2O_3 will transform the lattice oxygen of V_2O_5 into surface adsorption oxygen and capture the oxygen atom from V_2O_5 to generate As_2O_5. The formed As_2O_5 will bring forth dense oxide layers and cover the active sites, restraining the adsorption and activation of NH_3, finally reducing the activity of SCR catalyst. Peng et al. investigated the effects of arsenic over the SCR V_2O_5-WO_3/TiO_2 catalyst [18]. The results concluded that the arsenic species not only decreased the amount of Lewis acid sites but also decreased the strength of Brønsted acid sites. The decrease in Lewis acid sites results in a decrease in denitrification activity of the SCR catalysts because Lewis acids sites play an essential role in the formation of amide species from ammonia at a lower temperature. The amide species further react with gaseous NO and result in the the formation of intermediate NH_2NO and finally decompose to N_2 and H_2O [19].

Till now, several approaches, such as washing and thermal reduction, have been adopted for regeneration of the arsenic poisoned SCR catalysts. For the washing method, the alkaline solution can remove arsenic species from the catalyst and partially recover the catalytic activity. Unfortunately, this method is unable to eliminate the arsenic species completely and may also cause secondary poisoning of catalysts when some specific alkaline solutions (NaOH or KOH) are used [20]. Li et al. proposed the H_2 reduction method aiming at regenerating CeO_2-WO_3/TiO_2 catalyst [21]. This method improves the arsenic removal efficiency and facilitates the formation of NO_X adsorptive sites. However, it suffers from the defects of catalyst sintering and the following loss of active sites [22]. Therefore, it is essential to develop a more effective method to regenerate the arsenic-poisoned SCR catalyst.

†To whom correspondence should be addressed.
E-mail: qianglu@mail.ustc.edu.cn, qlu@ncepu.edu.cn

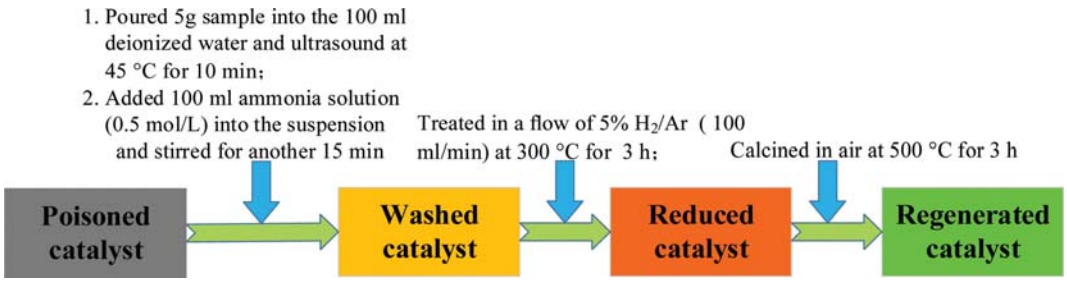

Fig. 1. Regeneration scheme of the poisoned catalyst.

In this study, a novel method is proposed to regenerate the arsenic poisoned commercial V_2O_5-MoO_3/TiO_2 type SCR catalyst, including the ammonia washing, H_2 reduction, and air calcination. The catalysts in each regeneration step were collected and subjected to activity tests and various characterizations. Finally, a tentative mechanism was proposed to elucidate the regenerative process of the arsenic poisoned catalyst.

EXPERIMENTAL

1. Catalyst Preparation and Regeneration

Both fresh and arsenic poisoned plate-type V_2O_5-MoO_3/TiO_2 catalysts were obtained from a coal-fired power plant in Inner Mongolia Province in China. Prior to the experiments, the catalyst samples were separated from the stainless steel meshes. Fresh catalyst was used as a reference sample. The poisoned catalyst was then regenerated by ammonia solution scrubbing, H_2 reduction, and air calcination, as shown in Fig. 1. H_2 reduction was performed by introducing 5% H_2/Ar (100 ml/min) at a heating rate of 10 °C/min from room temperature to 300 °C for 3 hours in horizontal reactor manufactured by Tianhong Lituo (Beijing Technology CO. LTD). The optimum calcination at 500 °C for 3 hours increased the surface area and Lewis acid sites and helped in the dispersion of active component over the catalyst surface, which corresponds to increase in mobility of lattice oxygen and recovers the redox reactions and finally contributes in an increase in activity of the SCR catalysts [23]. The catalyst obtained in each step was denoted by the regeneration method. All samples were crushed and sieved to obtained particles of 0.18-0.25 mm for characterization and activity measurements.

2. Activity Measurement

The catalytic activity was evaluated in a fixed-bed quartz reactor (I.D.=8 mm) based experimental equipment in Fig. 2. The inlet gas mixture contained 402 mg/Nm^3 NO, 228 mg/Nm^3 NH_3, 3% O_2, 5% H_2O, 500 mg/Nm^3 SO_2 and N_2 as the balance. The test temperature was 350 °C, the gas hourly space velocity (GHSV) was 180,000 h^{-1}. The concentrations of the outlet gases were continually monitored by an FT-IR spectrometer (German MRU company, model MGA5). The NO conversion efficiency of the catalysts was calculated as follows:

$$\eta = \frac{\varphi_{NO_{in}} - \varphi_{NO_{out}}}{\varphi_{NO_{in}}} \times 100\% \quad (1)$$

where η is the denitrification efficiency, $\varphi_{NO_{in}}$ and $\varphi_{NO_{out}}$ are the concentrations of NO in the flue gas before and after the catalytic reaction, respectively. The activity data were recorded under a 20-min-steady-state operation and the tests were replicated three times.

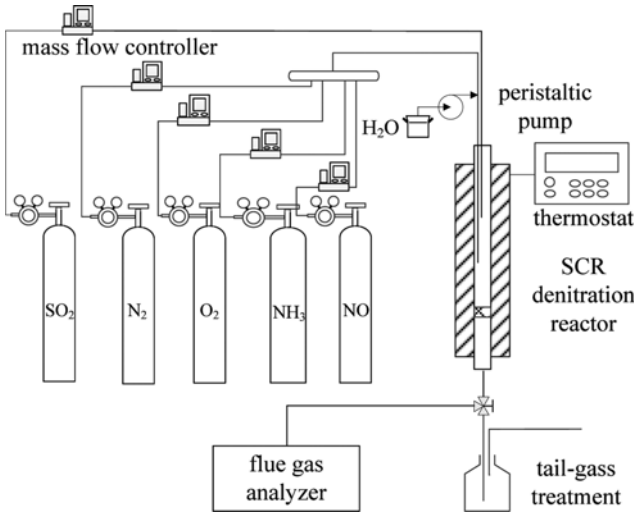

Fig. 2. Experimental setup to analyze the activity of the catalyst.

3. Catalyst Characterization

The elemental compositions of catalysts were analyzed by an X-ray fluorescence spectrometer (XRF-1800, Shimadzu, Japan). The Brunauer-Emmett-Teller (BET) surface area, total pore volume and average pore size of the catalysts were measured at −196 °C using a Micromeritics ASAP 2020 analyzer. Field emission scanning electron microscope (FE-SEM, Hitachi SU-8010) and the equipped energy dispersive spectroscopy (EDS) were used to identify the morphology and element distribution of the catalysts. X-ray photoelectron spectroscopy (XPS) experiments were performed on an ESCALAB 250 photoelectron spectrometer (ThermoFisher Scientific, USA) with an Al Kα (hv=1,486.6 eV) as the X-ray source, and the shift of binding energy was calibrated using the C1s level at 284.6 eV as an internal standard. Temperature programmed desorption (TPD) of NH_3 was carried out on a dynamic-flow gas sorption instrument (Quantachrome ChemBet 3000). Pyridine adsorption infrared spectrum (Py-IR) measurements were conducted on a Nicolet 6700 Spectrometer. Specifically, the sample disk was pretreated under vacuum at 350 °C for 2 h to remove physisorbed water. After cooling to room temperature, pyridine vapor was introduced into the IR cell for 1 h, and then wafer evacuations were performed at 150 °C for 0.5 h for spectral acquisition.

Table 1. The composition of the fresh, poisoned and regenerated catalysts (wt%)

Catalyst	Ti	V	Mo	As	Si	Al	S	K	Na	Fe	Ca	O
Fresh catalyst	52.85	1.49	3.06	-	0.57	0.20	-	0.01	0.11	0.15	0.39	41.17
Poisoned catalyst	51.38	1.45	3.02	1.48	1.18	0.56	0.09	0.04	0.10	0.29	0.36	40.05
Washed catalyst	52.39	1.35	2.90	0.58	1.18	0.56	0.03	0.02	0.08	0.27	0.33	40.31
Reduced catalyst	52.45	1.34	2.89	0.08	1.17	0.55	0.02	0.02	0.07	0.25	0.30	40.86
Regenerated catalyst	52.45	1.34	2.89	0.08	1.17	0.55	0.02	0.02	0.07	0.25	0.30	40.86

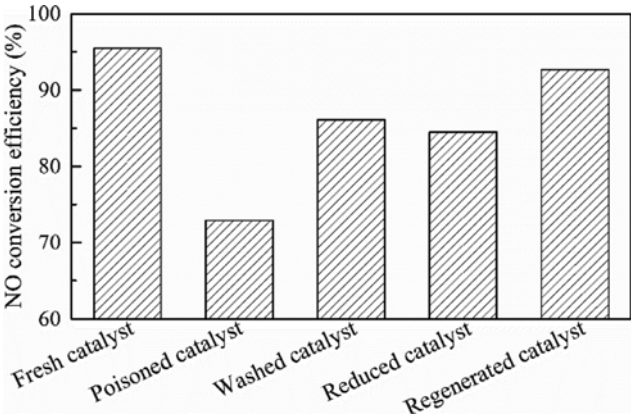

Fig. 3. The NO conversion efficiency of the fresh, poisoned and regenerated catalysts.

RESULTS AND DISCUSSION

1. Catalytic Activity

The elemental compositions of the fresh, arsenic poisoned and regenerated catalysts based on the XRF analysis are given in Table 1. The NH_3-SCR activities of these catalysts are shown in Fig. 3. The fresh catalyst was highly active, and the denitrification efficiency was up to 95.5% at 350 °C, in accordance with the V and Mo loadings of 1.49 wt% and 3.06 wt%. Note that no arsenic species were detected on the fresh catalyst, while a high percentage of As 1.48 wt% was found in the poisoned catalyst with a slight decrease of V and Mo loading, thus resulting in a sharp decrease of denitrification efficiency to 72.9%. It could be easily observed that the regeneration method had a significant effect on the compositions and activities of the catalyst samples. 60.8% As was removed in the ammonia washing process and the washed catalyst achieved 86.1% denitrification efficiency. It is notable that the V and Mo contents were further decreased to 1.35 wt% and 2.90 wt%, indicating that ammonia washing would cause a little loss of V_2O_5 and MoO_3.

Compared with the washed catalyst, a further remarkable decrease in As content of 0.08 wt% was observed in the reduced catalyst. However, corresponding denitrification efficiency was slightly decreased to 84.5%, indicating that H_2 reduction treatment would lead to the loss of active sites. This phenomenon will be explained by the following characterization results. After the last calcination stage, the catalyst exhibited a significant increase in the denitrification efficiency of 92.7%, close to the fresh catalyst. The results indicated a feasible regeneration of V_2O_5-MoO_3/TiO_2 catalyst by the proposed method.

In summary, the arsenic species were significantly decreased during the regeneration process, corresponding to the improvement of catalytic activity (Fig. 3). Although alkali metals, alkaline earth metals, and sulfur species would also cause deactivation of the catalyst, their content was relatively low and varied little in these catalysts. Hence, the enrichment of arsenic species on the catalyst mainly contributed to the deactivation of the catalyst, and the regeneration of the catalyst should mainly focus on the variation of arsenic species and active constituents of the catalysts.

Table 2. Surface areas and pore structures of the catalysts

Catalyst sample	S_{BET} (m^2/g)	D_{pore} (nm)	V_{pore} (cm^3/g)
Fresh catalyst	72.6	17.7	0.32
Poisoned catalyst	52.7	20.1	0.21
Washed catalyst	63.6	14.4	0.23
Reduced catalyst	64.4	15.7	0.25
Regenerated catalyst	69.7	16.7	0.25

2. Morphology and Structural Characteristics

Table 2 gives the textural properties of the fresh, poisoned and regenerated catalysts. Compared with the fresh catalyst, the BET surface area (S_{BET}) and pore volume (V_{pore}) of the poisoned catalyst reduced sharply, while the average pore diameter (D_{pore}) increased. This could be explained by the channel blocking effect [24]. In the regeneration process, the BET surface area and pore volume of the catalyst samples were improved after the successive ammonia washing, H_2 reduction, and air calcination treatment.

FE-SEM characterization was used to investigate the surface morphology of the catalysts, and the results are displayed in Fig. 4. As shown in the area circled by the red dotted line in Fig. 4(b), compared with the fresh catalyst, a significant number of porosities disappeared in the poisoned catalyst. Moreover, based on the EDS mapping results in Fig. 4(f), the arsenic species were observed uniformly dispersed on the surface of the poisoned catalyst. The results could be explained by the fact that the impurities, especially the gaseous arsenic species, diffused into the pore channels and clogged the micropores of the catalysts, thus resulting in the aggregation of particles and the loss of active sites [25]. Upon a successive of washing and thermal treatment, the particles were loosely stacked and formed a rough surface, demonstrating that the regeneration method could effectively eliminate the sediments deposited on the catalyst surface and recover the catalytic activity [26].

3. Surface Acidity

The NH_3 adsorption capacity of the catalysts, which plays a critical role in the SCR reaction, is found to be strongly correlated with the surface acidity of the catalysts [12,27]. NH_3-TPD analysis was performed to characterize the surface acidity of the five cata-

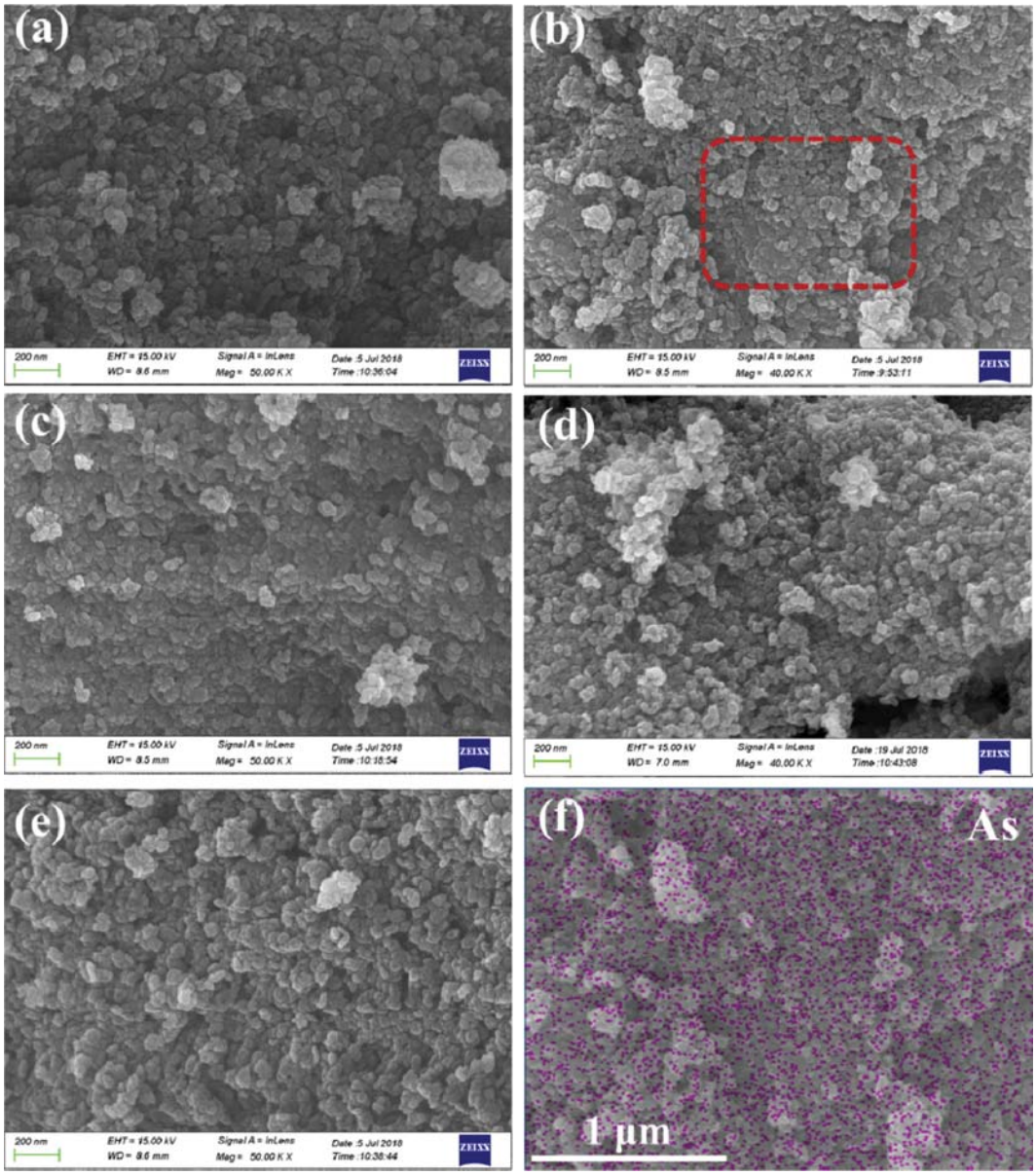

Fig. 4. FE-SEM images of (a) fresh catalyst, (b) poisoned catalyst, (c) washed catalyst, (d) reduced catalyst, (e) regenerated catalyst; EDS mapping (f) of the poisoned catalyst.

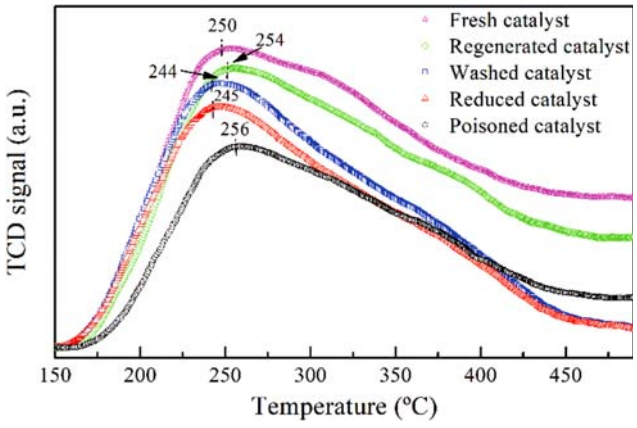

Fig. 5. NH_3-TPD profiles of the catalysts.

lyst samples (see Fig. 5). All catalysts exhibited an NH_3 desorption peak centered around 250 °C, which could be ascribed to the medium-strong acid sites of the catalysts [14]. Combining the BET surface area data in Table 2 with the profiles in Fig. 5, it could be found that as the BET surface area was significantly reduced, the desorption peak area was also reduced. The decrease in BET surface area was due to blockage of micropores on the catalyst surface and agglomeration of arsenic species, which also covered the acidic sites on the catalyst surface. When the catalyst was regenerated step by step, the blockage and agglomeration were gradually removed, and the BET surface area of the catalyst was also improved, which led to a gradual recovery of the acidic surface sites and an increase in the NH_3 desorption peak area. Note that after the reduction treatment, the content of As in the obtained reduced catalyst showed an obvious decline (Table 1), and the BET surface

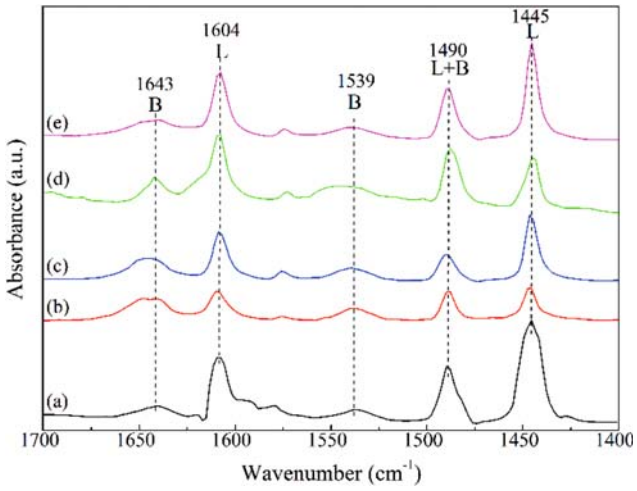

Fig. 6. Py-IR spectra of catalyst samples recorded at 150 °C. (a) fresh catalyst, (b) poisoned catalyst, (c) washed catalyst, (d) reduced catalyst, (e) regenerated catalyst.

area was also increased (Table 2), whereas the NH_3 absorption peak area of the reduced catalyst was decreased. This may be due to the imbalance of V valence states in the active phase caused by reduction treatment, which will be confirmed by XPS results.

Table 3. Py-IR semi-quantitative results of catalysts

Catalyst samples	C_{Lewis} (μmol/m^2)	$C_{Brönsted}$ (μmol/m^2)	C_{total} (μmol/m^2)
Fresh catalyst	3.16	0.40	3.56
Poisoned catalyst	0.72	0.67	1.39
Washed catalyst	2.10	0.48	2.58
Reduced catalyst	1.62	0.75	2.37
Regenerated catalyst	2.90	0.43	3.33

The nature of acid sites on different catalysts was further elucidated by Py-IR characterization (Fig. 6). The bands at 1,445 cm^{-1} and 1,604 cm^{-1} were assigned to Lewis acid (L) sites, and the bands at 1,539 cm^{-1} and 1,643 cm^{-1} were ascribed to the Brønsted acid (B) sites [28-30]. For a better presentation, the concentration of acid sites on the catalyst samples was evaluated by the peak areas of 1,539 cm^{-1} for Brønsted acid and 1,445 cm^{-1} for Lewis acid [31, 32]. As shown in Fig. 6 and Table 3, the Lewis acidity of the poisoned catalyst dropped sharply, whereas the Brønsted acidity in-

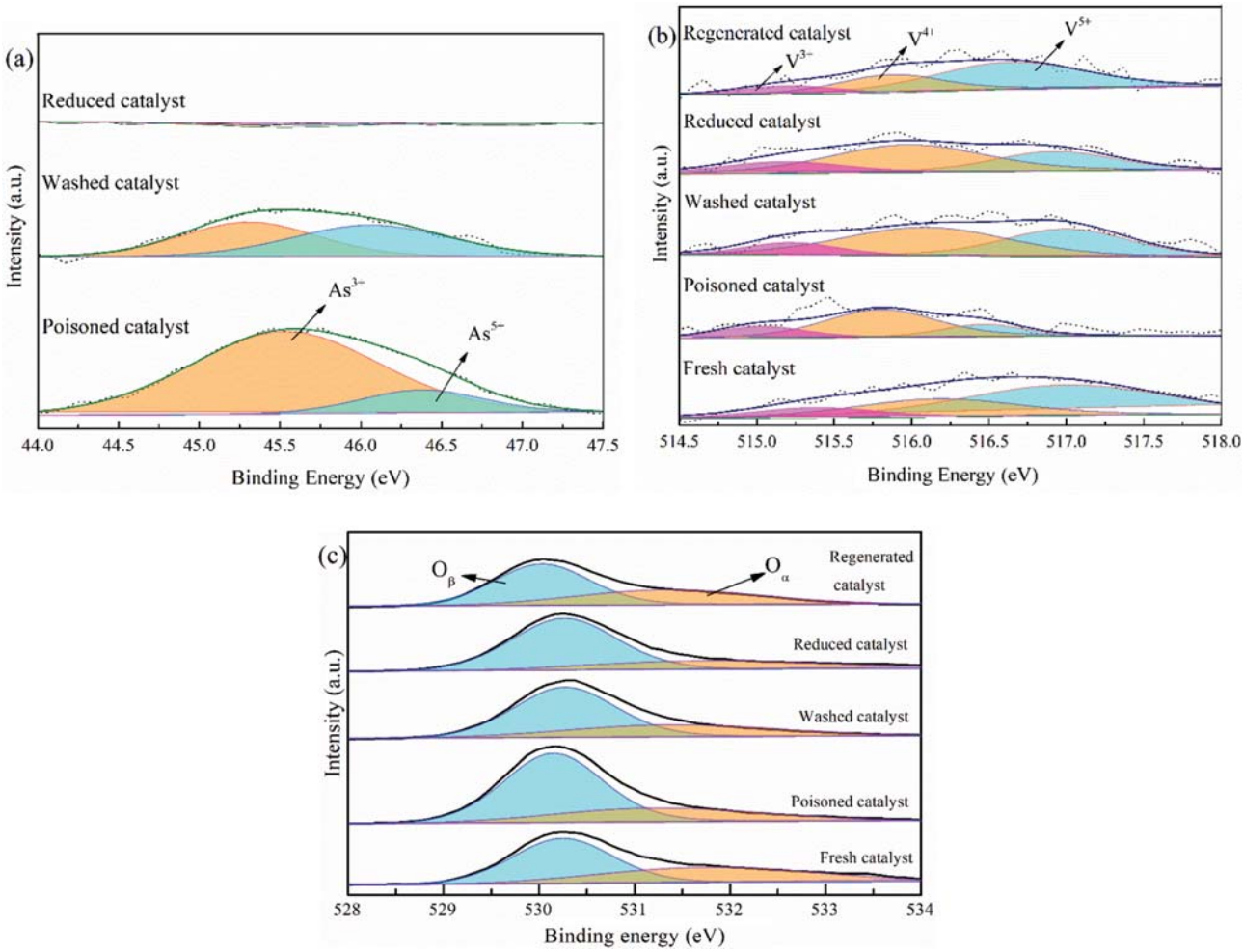

Fig. 7. XPS spectra of (a) As 3d, (b) V 2p3/2 and (c) O 1s for different catalysts.

creased slightly. This could be because arsenic species covered the V=O site and strongly inhibited the Lewis acidity [33]. In addition, the formed As-OH moieties would provide additional Brønsted acid sites and slightly increased the adsorption capacity of NH_3 [17]. Although a slight increase of the Brønsted acidity quantities was observed in the poisoned catalyst, the total acid sites in the sample were significantly weakened, which was the main reason for the deactivation of the poisoned catalyst. After ammonia washing, the Lewis acidity and total acidity increased, while a downtrend was observed on the Brønsted acidity. Thus, the washed catalyst exhibited a larger amount of entire acid sites than the poisoned catalyst, corresponding to a notable improvement of catalyst activity. It could be observed that the Lewis acidity of the reduced catalyst was suppressed, while its Brønsted acidity was enhanced, which could be explained by the dehydrating effect caused by the reduction treatment, i.e., V=O (Lewis acid sites) transformed into V-OH bond (Brønsted acid sites) [34]. Finally, the Lewis acidity and Brønsted acidity restored to the normal level through the calcination process, and the amount of total acid sites (3.33 μmol/m^2) on the regenerated catalyst reached a level similar to the fresh sample (3.56 μmol/m^2).

4. Chemical States Analysis

XPS technique was used to explore the surface information of atomic content and chemical environment in the catalysts. According to previous work, the peak located at 45.5 eV was attributed to As^{3+} and peak located at 46.5 eV was assigned to As^{5+} [18]. In Fig. 7(a) the concentration of As^{3+} in the poisoned catalyst was higher than that of As^{5+}, and after ammonia washing, the total concentration of arsenic on the catalyst decreased, but the proportion of As^{5+} increased. This may be attributable to the disproportionation reaction of As^{3+} under alkaline conditions producing As^{5+} and As^0 [35]. In Table 4, the total atomic concentration of As in the poisoned catalyst was 2.2 at% by XPS, and the As removal efficiencies after the washing and thermal treatment were 56.3% and 100%, respectively. Nevertheless, about 0.08 wt% As was detected in the regenerated catalyst through the XRF analysis. The different results between XPS and XRF analyses should be ascribed to the fact that XPS analysis only indicated the surface atomic content of the catalysts, which also suggested that arsenic species accumulated in the catalyst channels were more difficult to remove than the surface-exposed arsenic species [20].

Fig. 7(b) shows the high-resolution XPS spectra of the V 2p3/2. Three different valence states of vanadium species could be observed in all catalysts, i.e., V^{5+} centered at 516.4-517 eV, V^{4+} at 515.7-516.2 eV and V^{3+} at 515.2-515.7 eV. Combining the V 2p3/2 spectrum with Fig. 3, the catalytic performance of each catalyst fluctuated with the amount of high-valence vanadium (V^{5+}). This phenomenon seems to verify the importance of the high-valence vanadium on the SCR activity of the catalysts. According to the previous view, the acidity of the catalyst strongly depended on the specific $(V^{4+}+V^{3+})/V^{5+}$ ratio and played a decisive role in the adsorption capacity of ammonia [36]. For a detailed analysis of high- and low-valent vanadium, the casaXPS software with Shirley background was employed to quantify the relative amount of V^{5+}, V^{4+}, and V^{3+}. Compared with the fresh catalyst, the relative amount of V^{4+} and V^{3+} in the poisoned catalyst increased by 32.13% and 8.56%, respectively (Table 4), causing the disequilibrium of electron transfer among V^{3+}, V^{4+} and V^{5+} [36-38]. More importantly, the atomic concentration of active vanadium species (V^{5+}) decreased by 40.68% due to the coverage of arsenic species on the catalyst surface. These contributed greatly to the deactivation of the poisoned catalyst. After the washing process, the relative amount of V^{3+} and V^{4+} was slightly lowered by 7.98% and 10.4%, respectively, while the surface vanadium concentration increased from 0.54 at% to 0.85 at%. This could be explained by the fact that the ammonium solution removed most arsenic species on the catalyst surface. It is theoretically acknowledged that the catalytic activity should be improved with the further increase of surface vanadium concentration in the H_2 reduction process. However, the denitrification efficiency exhibited in the experiment decreased slightly. Note that in Fig. 7(b) and Table 4 the ratio of $(V^{4+}+V^{3+})/V^{5+}$ in the reduced catalyst increased, indicating that the high-valence vanadium was partially reduced to a low-valent state, destroying the valence balance of vanadium. Furthermore, the importance of the equilibrium of the vanadium valence state to the catalytic denitrification capacity was confirmed. The XPS results also supported our inference in the NH_3-TPD section and were consistent with the Py-IR results. Finally, when the $(V^{4+}+V^{3+})/V^{5+}$ ratio of the catalyst after calcination almost recovered to the level of the fresh catalyst, its catalytic activity also increased to a comparable level to fresh catalyst as expected.

The deconvoluted O 1s XPS spectra of the catalysts are plotted in Fig. 7(c). All catalysts showed two distinct sub-bands. The O 1s binding energy located at 529.7 eV could be assigned to lattice oxygen (denoted as O_β), and the binding energy at 531.2 eV belonged to surface adsorbed oxygen (denoted as O_α) [39]. It has been well established that the surface adsorbed oxygen was more active than the lattice oxygen due to its higher mobility [40]. Accordingly, the high percentage of $O_\alpha/(O_\alpha+O_\beta)$ would promote the oxidation of

Table 4. XPS results of the fresh, poisoned and regenerated catalysts

Catalyst sample	V 2p core level				O 1s core level			Surface atomic concentration (at%)	
	V^{5+} (%)	V^{4+} (%)	V^{3+} (%)	$(V^{4+}+V^{3+})/V^{5+}$	O_α (%)	O_β (%)	$O_\alpha/(O_\alpha+O_\beta)$	As	V
Fresh catalyst	59.53	28.34	12.12	0.67	45.75	54.25	0.45	-	1.02
Poisoned catalyst	18.85	60.47	20.68	4.30	30.09	69.91	0.30	2.2	0.54
Washed catalyst	37.23	50.07	12.70	1.68	36.04	63.96	0.36	0.96	0.85
Reduced catalyst	29.02	52.66	18.32	2.44	30.73	69.27	0.30	-	0.96
Regenerated catalyst	59.92	27.97	12.11	0.66	41.78	58.22	0.41	-	0.96

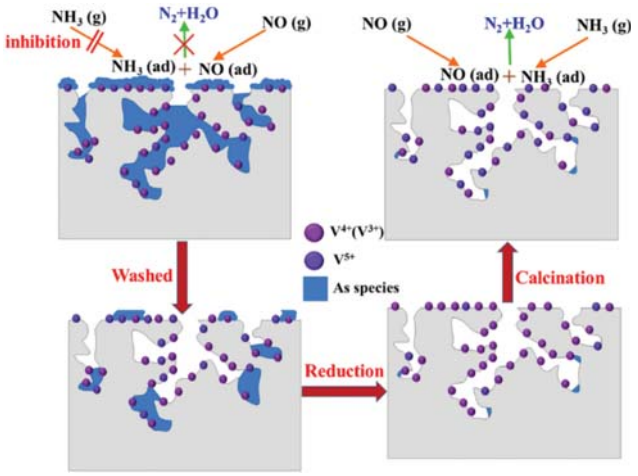

Fig. 8. Proposed regeneration mechanism of the arsenic poisoned catalyst.

NO, thus facilitating the "fast SCR" reaction, enhancing the SCR performance [21]. According to Table 4, the ratio of $O_\alpha/(O_\alpha+O_\beta)$ of the poisoned catalyst was lowest 0.30 and improved through the successive regenerating treatment. The only anomaly was that the ratio of reduced catalyst was lower than that of ammonia washed catalyst, which was due to the reaction of surface adsorbed oxygen with reducing agent H_2 to produce water.

PROPOSED REGENERATION MECHANISM

Based on the above results, it could be concluded that the deactivation of arsenic poisoned catalyst mainly resulted from the coverage of active vanadium sites and the valence imbalances. Our proposed regeneration method exhibited a remarkable superiority in improving the SCR performance. To interpret the effect of the treatment method on the property of the poisoned catalyst, a detailed regeneration mechanism was proposed. As shown in Fig. 8, the channels and surfaces of the poisoned catalyst were covered by the arsenic species, which was consistent with our BET surface area data. Moreover, the ratio of the active ingredient V^{5+} to total vanadium content in the catalyst was low. In this case, NO was difficult to react with NH_3. After the ammonium washing process, most of As could be removed, and V^{4+} (V^{3+}) was partially oxidized to form the active ingredient V^{5+}, which could be supported by XRF analysis and XPS results. Compared with other cleaning solutions, such as NaOH and KOH, the advantage of ammonia washing was the absence of secondary poisoning by the introduction of the alkali metal (Na or K) [20]. After that, the As residue, especially at the innermost part of the porous channels, was effectively removed by H_2 reduction (confirmed by XRF, As 3d spectrum of XPS), but the concentration of the Lewis acid site was lowered by the reduction of V^{5+} to V^{4+}(V^{3+}) (confirmed by V 2p3/2 spectrum of XPS). Finally, the post-calcination treatment promoted a further recovery of the $(V^{4+}+V^{3+})/V^{5+}$ ratio to the level of the fresh catalyst, which could be supported by XPS results. The main reactions occurring during ammonia washing, H_2 reduction, and air calcination are given below in the form of chemical equations.

Ammonia washing:

$$3As_2O_5+4NH_3\cdot H_2O=3As_2O_3+2N_2+10H_2O \quad (2)$$

$$As_2O_3+2NH_3\cdot H_2O=2As+N_2+5H_2O \quad (3)$$

H_2 reduction:

$$As_2O_3+3H_2=2As+3H_2O \quad (4)$$

$$As_2O_5+5H_2=2As+5H_2O \quad (5)$$

$$V_2O_5+H_2=2VO_2+H_2O \quad (6)$$

$$V_2O_5+2H_2=V_2O_3+2H_2O \quad (7)$$

$$V_2O_5+H_2+3H_2O=2V(OH)_4 \quad (8)$$

$$V_2O_5+2H_2+H_2O=2V(OH)_3 \quad (9)$$

Air calcination:

$$As_{(s)}\rightarrow As_{(g)} \quad (10)$$

$$4VO_2+O_2=2V_2O_5 \quad (11)$$

$$V_2O_3+O_2=V_2O_5 \quad (12)$$

$$4V(OH)_4+O_2=2V_2O_5+8H_2O \quad (13)$$

$$2V(OH)_3+O_2=V_2O_5+3H_2O \quad (14)$$

The removal efficiency of surface and total arsenic species was 100% and 94.8%, respectively, which was significantly higher than previously reported regeneration methods [20,21]. As a result, the regenerative process recovered the catalyst activity to more than 96% of the fresh catalyst. These characteristics indicated that the proposed method offered an efficient way to deal with the arsenic poisoned SCR catalyst.

CONCLUSION

Arsenic is an effective poison for V_2O_5-MoO_3/TiO_2 SCR catalysts, resulting in the catalyst deactivation in two aspects: reducing the number of Lewis acidity and disturbing the valence balance of V element. A novel method of ammonia washing - H_2 reduction - air calcination was developed to regenerate the arsenic poisoned catalyst from coal-fired power plants. The activity test results showed that the proposed method could recover to 96% primary activity of the fresh catalyst. In addition, the characterization results showed that the regeneration method removed the arsenic species effectively, recovered the $(V^{4+}+V^{3+})/V^{5+}$ ratio and increased the Lewis acidity and $O_\alpha/(O_\alpha+O_\beta)$ ratio, which improved the catalytic activity of the regenerated catalyst and made it similar to the fresh catalyst. It is believed that this technology could offer a feasible strategy for the regeneration of arsenic poisoned commercial SCR catalysts.

ACKNOWLEDGEMENTS

The authors thank the National key research and development plan (2018YFB0605103), National Natural Science Foundation of China (51576064), Beijing Nova Program (Z171100001117064), Beijing Natural Science Foundation (3172030), Grants from Fok Ying Tung Education Foundation (161051), State Key Laboratory of Catalytic Materials and Reaction Engineering, and Fundamental Research

Funds for the Central Universities (2018ZD08, 2016YQ05) for financial support.

REFERENCES

1. P. W. Seo, S. S. Kim and S. C. Hong, *Korean J. Chem. Eng.*, **27**, 1220 (2010).
2. L. T. Xu, S. L. Niu, C. M. Lu, D. Wang, K. Zhang and J. Li, *Korean J. Chem. Eng.*, **34**, 1576 (2017).
3. H. K. Feng, C. H. Wang and Y. Huang, *Korean J. Chem. Eng.*, **34**, 2832 (2017).
4. M. H. Hyeon and I. S. Nam, *Korean J. Chem. Eng.*, **18**, 725 (2001).
5. M. Lee, B. Ye, B. Jeong, H. Y. Chun, D. H. Lee, S. S. Park, H. Lee and H. D. Kim, *Korean J. Chem. Eng.*, **35**, 1988 (2018).
6. J. K. Lai and I. E. Wachs, *ACS Catal.*, **8**, 6537 (2018).
7. Y. Liu, J. Zhao and J. M. Lee, *ChemCatChem.*, **10**, 1499 (2018).
8. L. Xu, C. Wang, H. Chang, Q. Wu, T. Zhang and J. Li, *Environ. Sci. Technol.*, **52**, 7064 (2018).
9. H. Chang, C. Shi, M. Li, T. Zhang, C. Wang, L. Jiang and X. Wang, *Chin. J. Catal.*, **39**, 710 (2018).
10. X. Li, X. Li, T. Zhu, Y. Peng, J. Li and J. Hao, *Environ. Sci. Technol.*, **52**, 8578 (2018).
11. R. T. Guo, Q. S. Wang, W. G. Pan, Q. I. Chen, H. I. Ding, X. F. Yin, N. Z. Yang, C. Z. Lu, S. X. Wang and Y. C. Yuan, *J. Mol. Catal. A: Chem.*, **407**, 1 (2015).
12. C. H. Bartholomew, *Appl. Catal. A: Gen.*, **212**, 17 (2001).
13. Y. Zheng, A. D. Jensen and J. E. Johnsson, *Ind. Eng. Chem. Res.*, **43**, 941 (2004).
14. Z. Zhou, X. Liu, Z. Liao, H. Shao, Y. Hu, Y. Xu and M. Xu, *Chem. Eng. J.*, **304**, 121 (2016).
15. C. L. Senior, D. O. Lignell and A. F. Sarofim, *Combust. Flame.*, **147**, 209 (2006).
16. M. Kong, Q. Liu, X. Wang, S. Ren, J. Yang, D. Zhao, W. Xi and L. Yao, *Catal. Commun.*, **72**, 121 (2015).
17. Y. Peng, W. Si, X. Li, J. Luo, J. Li, J. Crittenden and J. Hao, *Appl. Catal. B: Environ.*, **181**, 692 (2016).
18. Y. Peng, J. H. Li, W. Z. Si, J. M. Luo, Y. Wang, J. Fu, X. Li, J. Crittenden and J. M. Hao, *Appl. Catal. B: Environ.*, **168**, 195 (2015).
19. S. Zhichun, W. Duan, W. Xiaodong and J. Yang, *J. Rare Earths*, **28**, 727 (2010).
20. X. Li, J. Li, Y. Peng, W. Si, X. He and J. Hao, *Environ. Sci. Technol.*, **49**, 9971 (2015).
21. X. Li, J. Li, Y. Peng, H. Chang, T. Zhang, S. Zhao, W. Si and J. Hao, *Appl. Catal. B: Environ.*, **184**, 246 (2016).
22. X. Li, J. Li, Y. Peng, X. Li, K. Li and J. Hao, *J. Phys. Chem. C.*, **120**, 18005 (2016).
23. N. Fang, J. Guo, S. Shu, H. Luo, J. Li and Y. Chu, *J. Taiwan Inst. Chem. E.*, **93**, 277 (2018).
24. X. Li, X. Li, J. Li and J. Hao, *J. Hazard. Mater.*, **318**, 615 (2016).
25. Y. Xue, Y. Zhang, Y. Zhang, S. Zheng, Y. Zhang and W. Jin, *Chem. Eng. J.*, **325**, 544 (2017).
26. Y. Yu, C. He, J. Chen, L. Yin, T. Qiu and X. Meng, *Catal. Commun.*, **39**, 78 (2013).
27. Y. Peng, J. Li, W. Shi, J. Xu and J. Hao, *Environ. Sci. Technol.*, **46**, 12623 (2012).
28. G. Busca and G. Ramis, *Appl. Surf. Sci.*, **27**, 114 (1986).
29. C. Martin, I. Martin, C. Delmoral and V. Rives, *J. Catal.*, **146**, 415 (1994).
30. E. P. Parry, *J. Catal.*, **2**, 371 (1963).
31. C. A. Emeis, *J. Catal.*, **141**, 347 (1993).
32. T. Barzetti, E. Selli, D. Moscotti, and L. Forni, *J. Chem. Soc, Faraday Trans.*, **92**, 1401 (1996).
33. Y. Peng, J. Li, W. Si, J. Luo, Q. Dai, X. Luo, X. Liu and J. Hao, *Environ. Sci. Technol.*, **48**, 13895 (2014).
34. A. Vittadini, M. Casarin and A. Selloni, *J. Phys. Chem. B.*, **109**, 1652 (2005).
35. M. Pušelj, Z. Ban and D. Grdenić, *Z. Anorg. Allg. Chem.*, **437**, 289 (1977).
36. P.-W. Seo, J.-Y. Lee, K.-S. Shim, S.-H. Hong, S.-C. Hong and S.-I. Hong, *J. Hazard. Mater.*, **165**, 39 (2009).
37. N. Y. Topsoe, H. Topsoe and J. A. Dumesic, *J. Catal.*, **151**, 226 (1995).
38. N. Y. Topsoe, J. A. Dumesic and H. Topsoe, *J. Catal.*, **151**, 241 (1995).
39. M. Shen, C. Li, J. Wang, L. Xu, W. Wang and J. Wang, *RSC Adv.*, **5**, 35155 (2015).
40. L. Chen, J. Li and M. Ge, *J. Phys. Chem. C.*, **113**, 21177 (2009).